The Journal of Chemical Physics

Factors that influence hydrogen binding at metal-atop sites

Cite as: J. Chem. Phys. **155**, 024703 (2021); https://doi.org/10.1063/5.0056774
Submitted: 13 May 2021 . Accepted: 15 June 2021 . Published Online: 09 July 2021

Huiling Zheng, Hao Li, Long Luo, Zhen Zhao, and Graeme Henkelman

The Journal of Chemical Physics ARTICLE scitation.org/journal/jcp

Factors that influence hydrogen binding at metal-atop sites

Cite as: J. Chem. Phys. 155, 024703 (2021); doi: 10.1063/5.0056774
Submitted: 13 May 2021 • Accepted: 15 June 2021 •
Published Online: 9 July 2021

Huiling Zheng,[1,2] Hao Li,[2,a)] Long Luo,[3] Zhen Zhao,[1,4] and Graeme Henkelman[2,b)]

AFFILIATIONS

[1] State Key Laboratory of Heavy Oil Processing, College of Science, China University of Petroleum-Beijing, Changping District, Beijing 102249, China
[2] Department of Chemistry and the Oden Institute for Computational Engineering and Sciences, University of Texas at Austin, Austin, Texas 78712-0231, USA
[3] Department of Chemistry, Wayne State University, Detroit, Michigan 48202, USA
[4] Institute of Catalysis for Energy and Environment, Shenyang Normal University, Shenyang 110034, China

[a)] **Present address:** Department of Physics, Technical University of Denmark, 2800 Kongens Lyngby, Denmark.
[b)] **Author to whom correspondence should be addressed:** henkelman@utexas.edu

ABSTRACT

The *d*-band model has proven to be effective for understanding trends in the chemisorption of various adsorbates on transition metal surfaces. However, hydrogen adsorption at the atop site of transition metals and their bimetallic alloy surfaces do not always correlate well with the *d*-band center of the adsorption site. Additionally, the *d*-band model cannot explain the disappearance of the local minima for H adsorption at the hollow site on the potential energy surface of 5*d* single-atom element doped Au and Ag(111) surfaces. Here, we use a simple model with factors, including the *d*-band center, filling of the *d*-band, renormalized adsorbate states, coupling matrix elements, and surface–adsorbate bond lengths, to correlate with the density functional theory calculated H binding energies on both mono- and bimetallic (111) surfaces. Our results suggest that H adsorption at metal-atop sites is determined by all these factors, not only by the *d*-band center. The strong adsorption of H at the atop sites of 5*d* metal surfaces can be explained by their lower repulsive contribution.

I. INTRODUCTION

Understanding the adsorption of adsorbates on surfaces is crucial to understanding catalysis. In the past few decades, models have been proposed for the chemisorption of simple adsorbates on transition metal surfaces.[1–8] The *d*-band model has proven effective for understanding trends in the adsorption energies of various adsorbates on transition metal surfaces.[5,6] The most simple form of this model correlates the *d*-band center, which is the average energy of *d*-electrons at an adsorption site, with the surface chemical reactivity.[1,5,6] The *d*-band model has been widely used to explain trends in the binding energy and reactivity of adsorbates on mono- and bimetallic surfaces[9–11] and has even been used to design new catalysts.[12–14] In general, for late transition metals, a *d*-band center closer to the Fermi level indicates a stronger bonding capacity to the adsorbate, which is due to the decreased filling of the adsorbate–metal antibonding states.[15] The binding energies of many adsorbates have shown a good correlation with the *d*-band center at a given adsorption site.[11,16,17]

The *d*-band model has limits, however, in that it uses a single averaged electronic property to describe the chemisorption and reactivity of an adsorption site. In past reports, some adsorbate–surface systems have been found to deviate from this model.[1,4,7,18] Studies based on these exceptions of the *d*-band model have established extended models by taking more factors into account,[1,2,4,18] including the *d*-band center (ε_d), the filling of the *d*-band (f),[1] and the coupling matrix element (V) between adsorbate states and the metal *d*-band.[1,4] Such models have been understood in terms of a two-step coupling between adsorbates and surface metals: the adsorbate states are first coupled with the *sp*-bands of the surface metal atom, and then, the renormalized adsorbate states are coupled with the surface metal *d*-bands. Since the coupling with *sp*-bands can be considered similar for transition metals, chemisorption on these surfaces primarily depends on the electronic interaction with

surface metal *d*-bands.[2] Hammer *et al.* used this model to analyze H_2 dissociation and CO chemisorption on various close-packed mono- and bimetallic surfaces.[1,4] Xin and Linic[18] further applied this model to explain the exception of the *d*-band theory for OH chemisorption on Pd and Pt skin alloys and a counter-intuitive trend between binding energies and the adsorbate–substrate bond length by analyzing the repulsion between the adsorbate states and the metal *d*-bands.

Hydrogen adsorption on transition metal surfaces is a key step in many chemical reactions, including hydrogenation, dehydrogenation, and hydrogenolysis.[19–26] Interestingly, hydrogen adsorption on transition metals still shows some unusual phenomena. For example, our previous studies found that single-atom 5*d* strong-binding transition metals (i.e., Pt and Ir) doped into Au, Ag, or Cu(111) have a favorable atop-site adsorption of H and no local minima for adsorption at the hollow or bridge sites (Fig. 1), while H prefers to bind at the threefold hollow or twofold bridge sites on most other mono- and bimetallic surfaces.[23,27,28] This atop-site adsorption leads to some unique catalytic activity[23,26,28] and even selectivity[22] on the catalytic surface. Meanwhile, while hollow-site adsorption on an alloy surface can be qualitatively correlated with the *d*-band center of the threefold alloy site,[29] the atop-site adsorption of H seems to deviate from the *d*- or dz^2-band centers of the single-atom site. Therefore, the current *d*-band model has limitations with respect to understanding trends of H-binding at metal-atop sites.

Motivated by these questions, we have re-analyzed the theory of atop-site adsorption of H on transition metal surfaces. First, we found that H adsorption energies on the atop site of 11 transition metals (Co, Ni, Ru, Rh, Pd, Os, Ir, Pt, Au, Ag, and Cu) and their bimetallic alloy surfaces are not well correlated with the *d*-band center of the site, and H adsorption at the atop site is strong on 5*d* metal surfaces. In addition, there are no local minima for H adsorption at the hollow site of 5*d* single-atom element doped Au and Ag(111) surfaces. Therefore, we analyzed additional factors that also contribute to the H binding energy at the surfaces. Our results show that H adsorption on transition metal surfaces depends not only on the *d*-band center but also on the size of *d*-orbitals of the surface metal atoms, renormalized adsorbate states, and adsorbate–metal bond lengths. We also found that the repulsive contribution to the *d*-band plays a key role in H adsorption since the *sp*-band contribution is similar on different metal surfaces. This model also helps with understanding the stronger atop-site adsorption on 5*d* metal surfaces originating from a reduced contribution from Pauli repulsion.

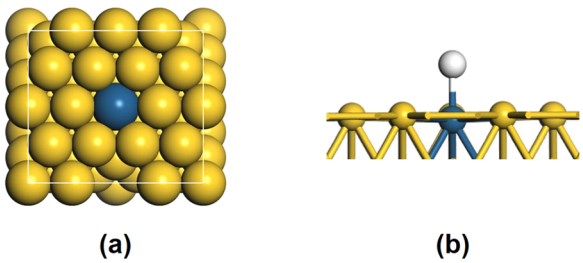

FIG. 1. Optimized configurations of (a) the Pt_1–Au_x(111) surface and (b) H adsorbed at the Pt-atop of Pt_1–Au_x(111). Yellow, blue, and white spheres represent Au, Pt, and H, respectively.

II. COMPUTATIONAL DETAILS

In this work, the Vienna *ab initio* simulation package (VASP)[30,31] was used to calculate all states with the electron exchange–correlation effect described by the Perdew–Burke–Ernzerh functional within the generalized gradient approximation (GGA-PBE).[32] Spin polarization was tested and used as needed, such as for the calculations of Ni(111) and Ni-based alloy surfaces and the H atom in vacuum. The projector augmented wave method was used to describe core–valence electron interaction.[33] A plane-wave basis with an energy cutoff of 400 eV was used to model the valence electrons.[34] All calculations were modeled on the slab (111) surface of a four-layer, 4 × 4 unit cell, face-centered cubic surface, with the bottom two atomic layers constrained in bulk positions. Geometries were considered relaxed when the forces on each atom decreased below 0.05 eV/Å. A vacuum gap of at least 12 Å in the *z*-direction was used to separate periodic images. A Monkhorst–Pack (3 × 3 × 1) *k*-point mesh was used for the Brillouin zone integration. For bimetallic alloys, we used late-transition metals X (X = Co, Ni, Ru, Rh, Pd, Os, Ir, and Pt) to substitute Au/Ag/Cu on an Au/Ag/Cu(111) surface, as shown in Fig. 1(a). The lattice constant of each surface was tuned between the lattice constants of X and Au/Ag/Cu following Vegard's law.[27]

H binding energies (E_b) were calculated using the following equation:

$$E_b = E_{tot} - E_{slab} - E_H, \quad (1)$$

where E_{tot} is the total energy of the combined system with H adsorbed at the atop site of the slab [Fig. 1(b)], E_{slab} is the energy of the bare slab, and E_H is the energy of an H atom in a vacuum. For comparison, we performed calculations on X–Au(111) (X = Co, Ni, Ru, Rh, Pd, Os, Ir, and Pt) surfaces using the revised PBE (RPBE)[35] functional; no significant difference was found in the adsorption energy and configuration. In the experimental benchmarking analysis by Wellendorff *et al.*,[36] PBE shows the closest values to experiments for H_2 dissociative adsorption energies compared to other methods (RPBE, BEEF-vdW,[37] etc.). Therefore, PBE was used in this study.

III. RESULTS AND DISCUSSION

Our density functional theory (DFT) calculations indicate that there are no local minima for H adsorption at the hollow site on the potential energy surface of 5*d* single-atom element doped Au and Ag(111) surfaces because H migrates spontaneously to the atop site of the 5*d* dopants (Os, Ir, and Pt), as shown in Fig. 2(a). However, H can stay at the hollow site on the 3*d* (Co and Ni) or 4*d* (Ru, Rh, and Pd) single-atom doped Au and Ag(111) surfaces, as shown in Fig. 2(b).

We first used the *d*-band center projected on the adsorption site to correlate with the DFT-calculated H binding energy at metal-atop sites on a number of mono- and bimetallic (111) surfaces [Fig. 3(a)]. It can be seen that H binding energies on most of these surfaces show a decreasing trend with an up-shift of the *d*-band center,

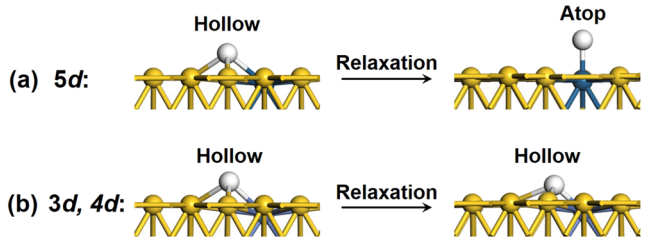

FIG. 2. Schematic illustration of H adsorption on single-atom doped Au and Ag(111) surfaces. The H adsorption site was initially placed at the threefold hollow. After DFT relaxation, H migrates to the atop site of the 5*d* dopants (Os, Ir, and Pt) (a), while it stays at the hollow site on the 3*d* (Co and Ni) or 4*d* (Ru, Rh, and Pd) single-atom doped Au and Ag(111) surfaces (b). White, blue, and yellow spheres represent H, the single-atom dopant, and the Au or Ag substrate, respectively.

which is qualitatively consistent with the *d*-band model.[5,6] However, there are still some non-negligible outliers that are far away from the fit lines. In addition, with a similar *d*-band center value, the order of H binding strength on different elemental periods is $5d > 4d > 3d$, which indicates that there are other factors that also affect the H binding at the metal-atop site. Additionally, the strong adsorption of H at the atop sites of 5*d* metal surfaces is consistent with the results of no stable adsorption at the hollow site shown in Fig. 2(a). Figure 3(b) shows that H binding becomes stronger as the surface–H distance increases on these close-packed surfaces, with the exceptions of monometallic Au, Ag, Cu, and Co. This result is opposite to the general understanding that stronger binding is correlated with shorter bond lengths[7] but similar with the OH adsorption on Pd and Pt skin alloys.[18] These unusual phenomena need to be explained by a model including factors besides the *d*-band center.

Before analyzing why the atop-site adsorption of H has outliers from the general understanding of the *d*-band model and the unusual phenomena of H adsorption at the atop site on 5*d* doped surfaces, we first discuss the two-step coupling between H and surface metals. First, the H 1*s* orbital couples with the *sp*-band of the surface metal atom. Since Al does not have *d*-electrons, we can use H adsorption on Al(111) to approximate the interaction between H and the *sp*-band of metal surfaces. This is similar to the analysis done in Refs. 1, 4, and 18. As shown in Figs. 4(a) and 4(b), when H is adsorbed on Al(111), the electronic state of H is broadened and shifts down in energy due to the hybridization of H and the surface metal broad *sp* band.[4,38] Furthermore, the presence of the *d*-bands in the transition metals leads to further coupling between the *d*-bands and the renormalized orbital of H, resulting in a lower energy level than the renormalized H orbital and metal *d*-band,[1,4,18] as shown in Fig. 4(c). Additionally, the total energy change is due to a competition between a hybridization energy gain and an orthogonalization energy cost.[4] As there are different features of *d*-bands between mono- and bimetallic surfaces,[39] we also show the projected density of states (PDOS) of H and the *d*-orbitals of the Pt atom of Pt_1–Au_x(111) [Figs. 4(e) and 4(f)]. These calculations show that although the alloys have a highly peaked DOS consisting of *d*-orbitals below the Fermi level with a higher energy relative to their monometallic counterparts, the interaction between the renormalized orbital of H and the *d*-orbital of the surface metal leads to a similar bonding interaction.

From the two-step coupling analysis, we can divide the H binding energy into the contribution from *sp*- and *d*-bands as follows:[40]

$$E_b = E_{sp} + E_d. \tag{2}$$

Since the *sp*-band of transition metals and their alloys are similarly broad, the contribution of the interaction between their *sp*-band and adsorbate orbital for the chemisorption can be approximately considered as a constant.[1,4,41] Therefore, we can consider the interaction of H and the substrate *sp*-band (E_{sp}) as an adjustable parameter in this model.[18]

Since H only has one 1*s* orbital interacting with the *d*-orbitals of the surface metal, we can write the following expression to describe the *d*-band contribution for H adsorption on transition

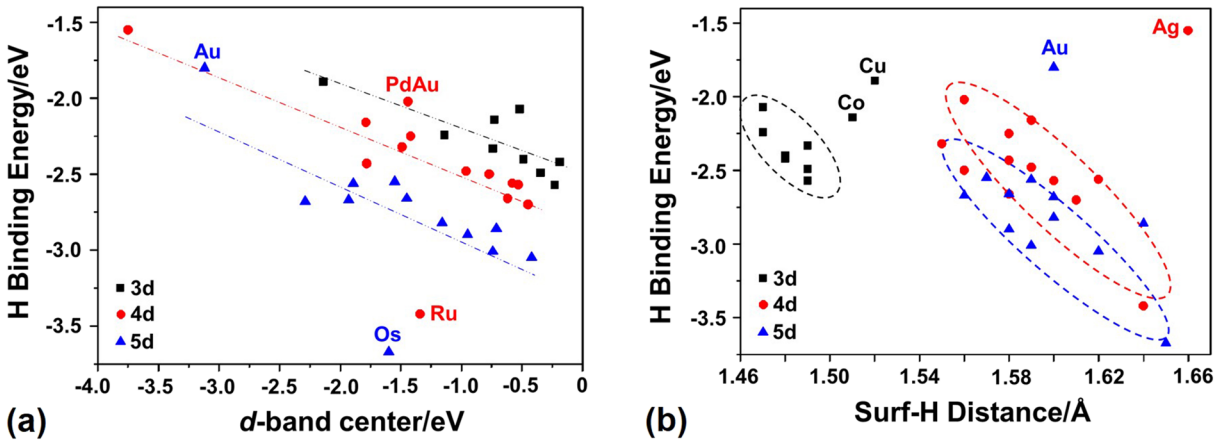

FIG. 3. (a) H binding energies on mono- and bimetallic (111) surfaces as a function of the *d*-band center of the adsorption site. Dashed lines are the linear trends. (b) H binding energies vs DFT-optimized surface–H distance.

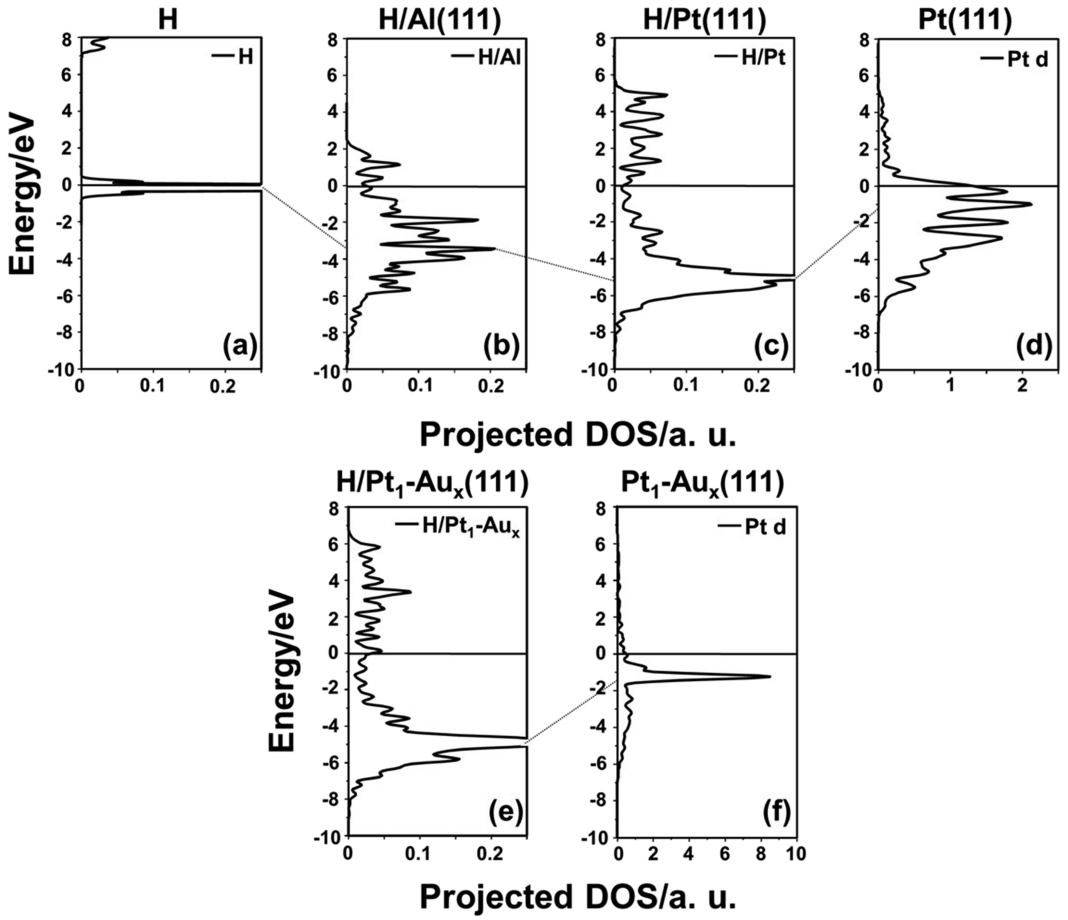

FIG. 4. (a) Projected density of states (PDOS) of H in vacuum. (b)–(e) PDOS on H adsorbed on the atop site of (b) Al(111), (c) Pt(111), and (e) Pt_1–Au_x(111). (d) and (f) PDOS on the *d*-orbitals of the surface Pt atom of (d) Pt(111) and (f) Pt_1–Au_x(111). The parallel black lines indicate the Fermi level, set to an energy of zero.

metal surfaces:[1,4,18]

$$E_d \approx -2\left[(1-f)\frac{V^2}{\varepsilon_d - \varepsilon_H} + (1+f)SV\right], \tag{3}$$

where the factor of 2 accounts for spin,[1] f and ε_d are the filling and center of the *d*-band at the adsorption site, and ε_H is the energy level of the renormalized H orbital formed after coupling with the *sp*-band of the surface metal atom. We took a value of −3.44 eV for the renormalized ε_H position on all these mono- and bimetallic (111) surfaces [Fig. 4(b)]. Finally, S and V are the overlap integral and coupling matrix element between the renormalized H orbital and *d*-bands of the surface metal atom, respectively. The first term in the parentheses represents the covalent attractive contribution due to the orbital hybridization, while the second term represents the repulsive contribution due to the orbital orthogonalization.[4,18]

The *d*-band center and filling were acquired by DFT calculations (Fig. 5). Since H has only one 1*s* orbital interacting with the *d*-orbitals of the surface metal, the *s*–*d* coupling matrix elements V_{sd} can be calculated as follows:[43]

$$V_{sd} = \eta_{sd\sigma}\frac{\hbar^2 r_d^{3/2}}{m d^{7/2}}, \tag{4}$$

where $\eta_{sd\sigma} = -3.11$[43] and $\hbar^2/m = 7.62$ eV/Å^2 are constants and r_d is the characteristic radius of the *d*-orbitals of a surface atom,[18,42] which we took from Wills' work,[42] as shown in Fig. 5. The bond length, d, between the adsorbed H and the surface metal atom was calculated using DFT. These factors are only dependent upon the surface metal atom that binds H. Now, we can introduce α and β as adjustable parameters so that we can write $V^2 \approx \beta V_{sd}^2$[1] and $S \approx -\alpha V$[4] and rewrite Eq. (3) as follows:

$$E_b \approx -2(1-f)\frac{\beta V_{sd}^2}{\varepsilon_d - \varepsilon_H} + 2\alpha\beta(1+f)V_{sd}^2 + E_{sp}, \tag{5}$$

where the attractive and repulsive contributions for E_d can be written, respectively, as follows:

$$E_{d-att} \approx -2(1-f)\frac{\beta V_{sd}^2}{\varepsilon_d - \varepsilon_H}, \tag{6}$$

Pure metals

f	V_{sd}^2	0.7	1.53	0.9	1.68	1	1
M		Co		Ni		Cu	
r_d		ε_d					
0.7	2.26	0.9	2.46	0.9	2.41	1	1.27
Ru		Rh		Pd		Ag	
1.05	-1.34	0.99	-1.78	0.94	-1.49	0.89	-3.75
0.7	2.70	0.9	2.92	0.9	3.12	1	2.39
Os		Ir		Pt		Au	
1.13	-1.60	1.08	-2.29	1.04	-1.93	1.01	-3.12

(a)

M_1-Au_x alloys

f	V_{sd}^2	0.7	1.76	0.9	1.50
M		Co		Ni	
r_d		ε_d			
0.7	2.69	0.8	2.69	0.9	2.30
Ru		Rh		Pd	
1.05	-0.53	0.99	-0.77	0.94	-1.44
0.6	3.22	0.8	3.19	0.9	2.98
Os		Ir		Pt	
1.13	-0.53	1.08	-0.95	1.04	-1.55

(b)

M_1-Ag_x alloys

f	V_{sd}^2	0.8	1.68	0.9	1.43
M		Co		Ni	
r_d		ε_d			
0.7	2.58	0.8	2.46	0.9	2.11
Ru		Rh		Pd	
1.05	-0.45	0.99	-0.62	0.94	-1.42
0.7	3.07	0.8	3.06	0.9	2.86
Os		Ir		Pt	
1.13	-0.42	1.08	-0.74	1.04	-1.45

(c)

M_1-Cu_x alloys

f	V_{sd}^2	0.8	1.68	0.9	1.37
M		Co		Ni	
r_d		ε_d			
0.7	2.46	0.8	2.36	0.9	2.02
Ru		Rh		Pd	
1.05	-0.45	0.99	-0.62	0.94	-1.42
0.7	2.82	0.8	2.92	0.9	2.73
Os		Ir		Pt	
1.13	-0.42	1.08	-0.74	1.04	-1.45

(d)

FIG. 5. Periodic Table of the late 3*d*, 4*d*, and 5*d* (a) transition metals and the corresponding single-atom alloys: (b) M_1–Au_x, (c) M_1–Ag_x, and (d) M_1–Cu_x. Upper-left corner: filling of the *d*-band projected on the surface metal atom. Upper-right corner: the square of the *s*–*d* coupling matrix element V_{sd}^2 (normalized to 1 for Cu). Lower-left corner: the characteristic radius of the *d*-orbitals of the surface atom, using data from Wills' work.[42] Lower-right corner: the *d*-band center of the surface atom. All energies are in eV, and distances are in Å.

$$E_{d-re} \approx 2\alpha\beta(1+f)V_{sd}^2. \tag{7}$$

The parameter β determines the slope, while E_{sp} determines the intercept of the fitted line. According to the discussion in Fig. 3, it is reasonable to use different α values for metal elements of each period.[18] Figures 6(a)–6(d) show the comparison between the model-predicted and DFT-calculated H binding energies on mono- and bimetallic surfaces. The adjustable parameters were acquired by minimizing the residual between model-predicted and DFT-calculated H binding energies, which are listed in Table I. It can be seen that there is a good agreement between the predicted and DFT-calculated binding energies by a constant value of α for the surface-active metal elements of each period. Similar to Xin's result, this model with adjustable parameters α and E_{sp} can capture the OH adsorption well on Pd and Pt skin alloys with different subsurface atoms (3*d*, 4*d*, or 5*d*).[18] The difference is that this model can also quantitatively explain H adsorption at the atop site of mono- and bimetallic (111) alloy surfaces.

To analyze the general applicability of this model, we used the same values of α (for each period), β, and E_{sp} for all these surfaces to compare with the DFT-calculated H binding energies [Fig. 6(e)]. The values of adjustable parameters are listed in Table I, and their magnitude is in the same order as in the works of Hammer[4] and Nørskov.[44] It can be seen that there is a good linear correlation between the predicted and DFT-calculated H binding energies on the mono- and bimetallic surfaces, with an R^2 value of 0.80. We then used the one-at-a-time method to perform a sensitivity analysis of our model. We assigned data in Fig. 6(e) as the base case, changed one model input by 10%, and then, obtained the sensitivity indices of all the model input, as shown in Fig. S1. It can be seen that the model is the most sensitive to the surface–H distance and E_{sp}, while it is the least sensitive to ε_d and α. The sensitivity index order is $d > E_{sp} > f = r_d > \varepsilon_H > V_{sd}^2 = \beta > \alpha > \varepsilon_d$. Additionally, from this model, we can see that the *d*-band center of the surface metal atom is not the only factor affecting H adsorption at the metal-atop site, and it is also affected by the size of the *d*-orbitals of the surface metal atoms, the renormalized adsorbate states, and the adsorbate–metal bond length. Compared with the *d*-band model with only one descriptor, the H-binding model with multiple descriptors can directly predict the binding energies and is suitable for both mono- and bimetallic systems.

The size of the *d*-orbitals depends only on the metal atom, and the renormalized adsorbate states are similar for all transition metals.[1,4,41] Therefore, we can analyze how the adsorbate–metal bond length affects the binding energy. From Eq. (4), V_{sd} is inversely proportion to $d^{7/2}$. However, the presence of r_d in Eq. (4) makes the relationship more complicated. We plotted V_{sd}^2 as a function of the surface–H distance in Fig. 7(a). It can be seen that V_{sd}^2 decreases with an increase in the surface–H distance for the same surface metal atom with different substrates, and the relationship is almost linear. From Eq. (7), the repulsive term is proportional to V_{sd}^2 [Fig. 7(b)]. Therefore, we can explain the unusual phenomena shown in Fig. 3(b). As the surface–H distance increases, V_{sd}^2 decreases, and then, the repulsive contribution for E_d decreases as well. Weaker repulsion between the H renormalized states and the *d*-orbitals of the surface metal atom makes the H binding stronger. This is similar to OH adsorption on Pd and Pt skin alloys.[18] The outliers (Au, Ag, and Cu) do not have an attractive contribution for E_d, leading to weaker H binding. Co is also an outlier but can be explained in another way: the energy level of the *d*-band center of Co is lower than those of Co-sites on Co-based alloys, which makes the attractive term in Eq. (6) higher, resulting in weaker H binding.

To further understand the presence of the outliers in Fig. 3(a) and the strong adsorption on 5*d* single-atom element doped surfaces, we analyze the components of the H binding energy and the contribution from the *d*-band. From Eqs. (2) and (3), we plot these components in Fig. 8. It can be seen that the contribution from the *sp*-band is dominant in H adsorption. In addition to the broad *sp*-bands of these metals, the significant repulsive contributions to E_d counteract most of the attraction, leading to smaller contributions of the *d*-band to H adsorption. The surface metal atoms with high *d*-band fillings show a lower attraction contribution to E_d and a less significant *d*-band contribution to H binding energies after being counteracted by the repulsive contributions. We can also see that the values of E_d for Au, Ag, and Cu are positive. We can

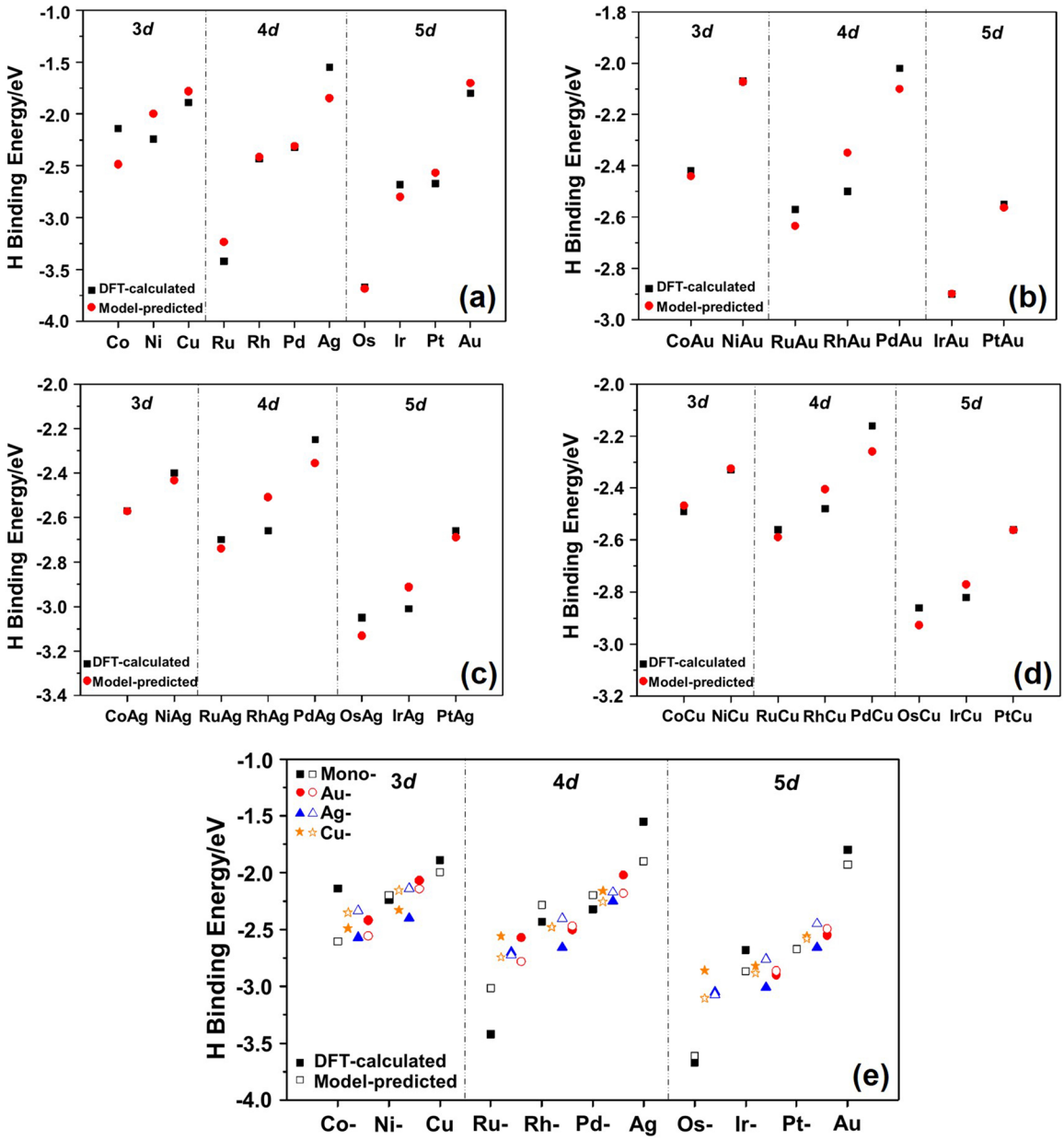

FIG. 6. Model-predicted vs DFT-calculated H binding energies on (a) monometallic (111) surfaces, the dopant atop sites of (b) Au-, (c) Ag-, and (d) Cu-based bimetallic (111) surfaces, and (e) all mono- and bimetallic (111) surfaces.

TABLE I. The values of adjustable parameters on monometallic and bimetallic (111) alloys.

Adjustable parameters		Pure metals	Au-based bimetallic	Ag-based bimetallic	Cu-based bimetallic	All mono- and bimetallic
α	$3d$	0.020	0.025	0.016	0.010	0.015
	$4d$	0.010	0.029	0.032	0.032	0.022
	$5d$	0.012	0.006	0.008	0.012	0.010
β		2.24	1.71	1.35	1.32	1.90
E_{sp}		−1.96	−2.14	−2.42	−2.26	−2.11

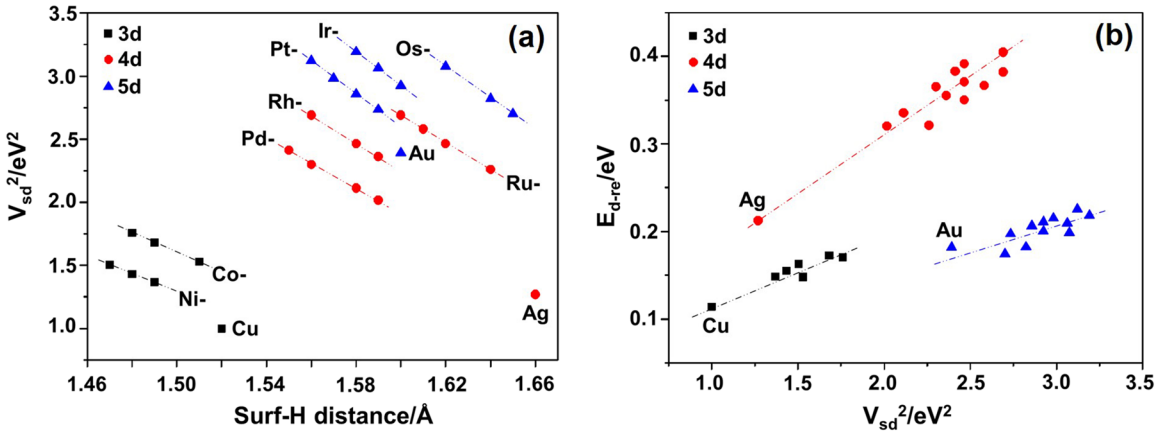

FIG. 7. (a) V_{sd}^2 as a function of surface–H distance. (b) Repulsive contribution E_{d-re} for E_d as a function of V_{sd}^2 on mono- and bimetallic (111) surfaces.

understand this from Eq. (6) that the attractive term is zero because of their fully filled *d*-band. Therefore, they only have repulsive contributions for E_d, resulting in weaker adsorption compared with the other monometallic surfaces. In addition, the strong atop-site adsorption of strong-binding 5*d* transition metals [Fig. 3(a)] can be explained by the lower repulsive contribution to E_d, compared to those 4*d* metals. We can see that Au/Ag shows the weakest H binding compared to other monometallics in Fig. 6(a), while the 4*d* and 5*d* monometallics have stronger H binding. The hollow-site adsorption on single-atom doped Au/Ag surfaces has H binding with two Ag/Au atoms and one dopant atom. When the three surface metal atoms bound to H show similar binding capacities, the hollow-site adsorption configuration of H is stable. However, the small repulsive contribution of the 5*d* dopants leads to a stronger binding, which helps 5*d* dopants strongly abstract H to their atop sites. This helps explain the disappearance of the local minima for H adsorption at

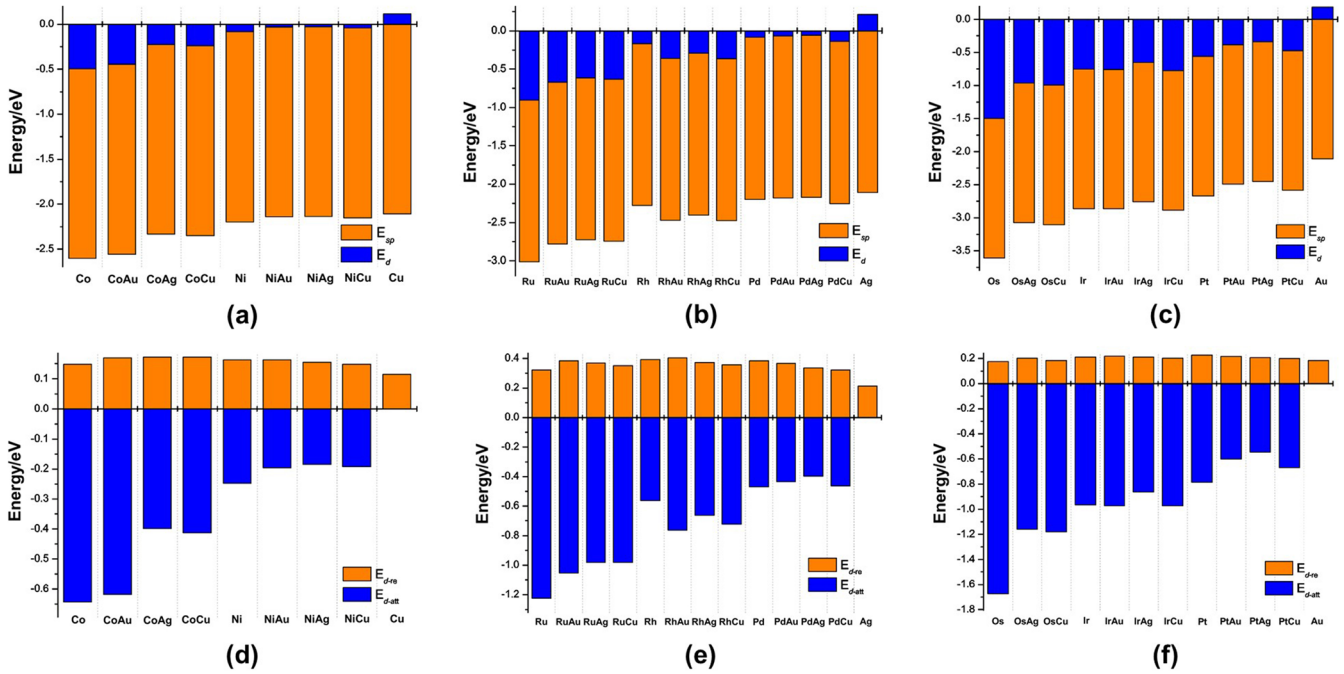

FIG. 8. Comparison of the contribution of *sp*- (orange) and *d*-bands (dark blue) to the H binding energy on mono- and bimetallic surfaces of (a) 3*d*, (b) 4*d*, and (c) 5*d* transition metals. Comparison of the contribution of attraction (dark blue) and repulsion (orange) to E_d on mono- and bimetallic surfaces for (d) 3*d*, (e) 4*d*, and (f) 5*d* transition metals.

the hollow site on the potential energy surface of 5*d* single-atom element doped Au and Ag (111) surfaces [Fig. 2(a)]. However, because the adjustable parameters (α and β) cannot be measured directly,[1,4,18] we can only qualitatively conclude that the repulsion contribution plays a key role in H adsorption at the metal-atop site of mono- and bimetallic transition metal surfaces, which also makes those outliers deviate from the general trends with the *d*-band model and the strong binding on 5*d* single-atom element doped surfaces.

IV. CONCLUSIONS

In summary, we have shown that the atop-site adsorption of H on 11 transition metals (Co, Ni, Ru, Rh, Pd, Os, Ir, Pt, Au, Ag, and Cu) and their bimetallic alloy surfaces are not well correlated with the *d*-band center of the adsorption site. The H adsorption at the atop site is strong, and there are no local minima for H adsorption at the fcc site on the potential energy surface of 5*d* single-atom element doped surfaces. We used a model with multiple factors, including the *d*-band center and filling, renormalized adsorbate states, coupling matrix element, and adsorbate–substrate bond length, to understand the DFT-calculated H binding energies on both the mono- and bimetallic (111) alloy surfaces. Our results indicate that H binding at metal-atop sites is affected by all these factors, not only by the *d*-band center. From this model, we can understand the significantly different repulsion between the renormalized adsorbate states and the *d*-band of the adsorption site. The outliers in the *d*-band correlation and the strong adsorption of H at the atop-site of 5*d* metal surfaces can also be explained by their significantly different repulsive component.

SUPPLEMENTARY MATERIAL

See the supplementary material for a sensitivity analysis determining the most important parameters in our H-binding model.

AUTHORS' CONTRIBUTIONS

H.Z. and H.L. contributed equally to this work.

ACKNOWLEDGMENTS

The authors are grateful for financial support from the National Natural Science Foundation of China (Grant Nos. 91845201 and U1908204) and the China Scholarship Council (Grant No. 201806440058). The work at UT Austin was supported by the Welch Foundation (Grant No. F-1841) and the Texas Advanced Computing Center.

DATA AVAILABILITY

The data that support the findings of this study are available from the corresponding author upon reasonable request.

REFERENCES

[1] B. Hammer and J. K. Nørskov, Surf. Sci. **343**, 211 (1995).
[2] A. Ruban, B. Hammer, P. Stoltze, H. L. Skriver, and J. K. Nørskov, J. Mol. Catal. A: Chem. **115**, 421 (1997).
[3] B. Hammer and M. Scheffler, Phys. Rev. Lett. **74**, 3487 (1995).
[4] B. Hammer, Y. Morikawa, and J. K. Nørskov, Phys. Rev. Lett. **76**, 2141 (1996).
[5] J. K. Nørskov, Prog. Surf. Sci. **38**, 103 (1991).
[6] B. Hammer and J. K. Nørskov, Nature **376**, 238 (1995).
[7] H. Xin, A. Vojvodic, J. Voss, J. K. Nørskov, and F. Abild-Pedersen, Phys. Rev. B: Condens. Matter Mater. Phys. **89**, 115114 (2014).
[8] F. Calle-Vallejo, J. I. Martínez, J. M. García-Lastra, J. Rossmeisl, and M. T. M. Koper, Phys. Rev. Lett. **108**, 116103 (2012).
[9] E. Toyoda, R. Jinnouchi, T. Hatanaka, Y. Morimoto, K. Mitsuhara, A. Visikovskiy, and Y. Kido, J. Phys. Chem. C **115**, 21236 (2011).
[10] O. Skoplyak, M. A. Barteau, and J. G. Chen, J. Phys. Chem. B **110**, 1686 (2006).
[11] C. Lu, I. C. Lee, R. I. Masel, A. Wieckowski, and C. Rice, J. Phys. Chem. A **106**, 3084 (2002).
[12] V. Stamenkovic, B. S. Mun, K. J. J. Mayrhofer, P. N. Ross, N. M. Markovic, J. Rossmeisl, J. Greeley, and J. K. Nørskov, Angew. Chem. **118**, 2963 (2006).
[13] J. K. Nørskov, T. Bligaard, J. Rossmeisl, and C. H. Christensen, Nat. Chem. **1**, 37 (2009).
[14] V. R. Stamenkovic, B. S. Mun, M. Arenz, K. J. J. Mayrhofer, C. A. Lucas, G. Wang, P. N. Ross, and N. M. Markovic, Nat. Mater. **6**, 241 (2007).
[15] J. K. Nørskov, F. Abild-Pedersen, F. Studt, and T. Bligaard, Proc. Natl. Acad. Sci. U. S. A. **108**, 937 (2011).
[16] L. G. M. Pettersson and A. Nilsson, Top. Catal. **57**, 2 (2014).
[17] L. A. Kibler, A. M. El-Aziz, R. Hoyer, and D. M. Kolb, Angew. Chem., Int. Ed. **44**, 2080 (2005).
[18] H. Xin and S. Linic, J. Chem. Phys. **132**, 221101 (2010).
[19] P. Nordlander, S. Holloway, and J. K. Nørskov, Surf. Sci. **136**, 59 (1984).
[20] P. Ferrin, S. Kandoi, A. U. Nilekar, and M. Mavrikakis, Surf. Sci. **606**, 679 (2012).
[21] J. Greeley and M. Mavrikakis, J. Phys. Chem. B **109**, 3460 (2005).
[22] H. Li, C. Yan, H. Guo, K. Shin, S. M. Humphrey, C. J. Werth, and G. Henkelman, ACS Catal. **10**, 7915 (2020).
[23] H. Guo, H. Li, K. Jarvis, H. Wan, P. Kunal, S. G. Dunning, Y. Liu, G. Henkelman, and S. M. Humphrey, ACS Catal. **8**, 11386 (2018).
[24] H. Li, W. Chai, and G. Henkelman, J. Mater. Chem. A **7**, 23868 (2019).
[25] E. J. Evans, H. Li, W.-Y. Yu, G. M. Mullen, G. Henkelman, and C. B. Mullins, Phys. Chem. Chem. Phys. **19**, 30578 (2017).
[26] H. Guo, H. Li, D. Fernandez, S. Willis, K. Jarvis, G. Henkelman, and S. M. Humphrey, Chem. Mater. **31**, 10225 (2019).
[27] H. Li, K. Shin, and G. Henkelman, J. Chem. Phys. **149**, 174705 (2018).
[28] L. Luo, Z. Duan, H. Li, J. Kim, G. Henkelman, and R. M. Crooks, J. Am. Chem. Soc. **139**, 5538 (2017).
[29] H. Li, E. J. Evans, C. B. Mullins, and G. Henkelman, J. Phys. Chem. C **122**, 22024 (2018).
[30] G. Kresse and J. Furthmüller, Phys. Rev. B: Condens. Matter Mater. Phys. **54**, 11169 (1996).
[31] G. Kresse and J. Furthmüller, Comput. Mater. Sci. **6**, 15 (1996).
[32] J. P. Perdew, K. Burke, and M. Ernzerhof, Phys. Rev. Lett. **77**, 3865 (1996).
[33] P. E. Blöchl, Phys. Rev. B **50**, 17953 (1994).
[34] B. J. Morgan and G. W. Watson, J. Phys. Chem. C **113**, 7322 (2009).
[35] B. Hammer, L. B. Hansen, and J. K. Nørskov, Phys. Rev. B: Condens. Matter Mater. Phys. **59**, 7413 (1999).
[36] J. Wellendorff, T. L. Silbaugh, D. Garcia-Pintos, J. K. Nørskov, T. Bligaard, F. Studt, and C. T. Campbell, Surf. Sci. **640**, 36 (2015).
[37] J. Wellendorff, K. T. Lundgaard, A. Møgelhøj, V. Petzold, D. D. Landis, J. K. Nørskov, T. Bligaard, and K. W. Jacobsen, Phys. Rev. B: Condens. Matter Mater. Phys. **85**, 235149 (2012).
[38] J. K. Nørskov, Rep. Prog. Phys. **53**, 1253 (1990).
[39] H. Thirumalai and J. R. Kitchin, Top. Catal. **61**, 462 (2018).
[40] B. Hammer, Top. Catal. **37**, 3 (2006).
[41] E. Santos, A. Lundin, K. Pötting, P. Quaino, and W. Schmickler, Phys. Rev. B: Condens. Matter Mater. Phys. **79**, 235436 (2009).
[42] J. M. Wills and W. A. Harrison, Phys. Rev. B **28**, 4363 (1983).
[43] W. A. Harrison and S. Froyen, Phys. Rev. B **21**, 3214 (1980).
[44] J. K. Nørskov, J. Chem. Phys. **90**, 7461 (1989).